The Plant Cell, Vol. 26: 325–339, January 2014, www.plantcell.org

Arabidopsis Microtubule-Destabilizing Protein 25 Functions in Pollen Tube Growth by Severing Actin Filaments[W]

Tao Qin,[1] Xiaomin Liu,[1] Jiejie Li, Jingbo Sun, Leina Song, and Tonglin Mao[2]

State Key Laboratory of Plant Physiology and Biochemistry, Department of Plant Sciences, College of Biological Sciences, China Agricultural University, Beijing 100193, China

ORCID ID: 0000-0003-3014-5350 (T.M.)

The formation of distinct actin filament arrays in the subapical region of pollen tubes is crucial for pollen tube growth. However, the molecular mechanisms underlying the organization and dynamics of the actin filaments in this region remain to be determined. This study shows that *Arabidopsis thaliana* MICROTUBULE-DESTABILIZING PROTEIN25 (MDP25) has the actin filament–severing activity of an actin binding protein. This protein negatively regulated pollen tube growth by modulating the organization and dynamics of actin filaments in the subapical region of pollen tubes. *MDP25* loss of function resulted in enhanced pollen tube elongation and inefficient fertilization. MDP25 bound directly to actin filaments and severed individual actin filaments, in a manner that was dramatically enhanced by Ca^{2+}, in vitro. Analysis of a mutant that bears a point mutation at the Ca^{2+} binding sites demonstrated that the subcellular localization of MDP25 was determined by cytosolic Ca^{2+} level in the subapical region of pollen tubes, where MDP25 was disassociated from the plasma membrane and moved into the cytosol. Time-lapse analysis showed that the F-actin-severing frequency significantly decreased and a high density of actin filaments was observed in the subapical region of *mdp25-1* pollen tubes. This study reveals a mechanism whereby calcium enhances the actin filament–severing activity of MDP25 in the subapical region of pollen tubes to modulate pollen tube growth.

INTRODUCTION

Sperm cells of flowering plants are nonmotile and are delivered via the haploid male gametophyte (pollen) to the female gametophytes (embryo sacs). Pollen grains germinate and produce pollen tubes on the stigma of the pistil, which grow through the style into the transmitting tissue and are then guided to the micropylar opening of the ovules (Kägi and Gross-Hardt, 2007; Crawford and Yanofsky, 2008). When pollen tubes reach the female gametophyte, their growth is arrested and the tube tips rupture to release the sperm cells (Huck et al., 2003; Boisson-Dernier et al., 2009). The regulation of pollen tube growth is necessary for the purpose of double fertilization. The growth of the pollen tube is supported by rapid trafficking of vesicles to deliver membrane and cell wall components to the tips (Picton and Steer, 1983; Lee and Yang, 2008; Yang, 2008). The actin cytoskeleton plays a crucial function in multiple plant cellular processes, including regulation of the cytoplasmic streaming and organelle movements. Pharmacological treatments and genetic disturbances of actin organization and dynamics revealed that the actin cytoskeleton is a major regulator of pollen tube growth (Chen et al., 2002; Cheung and Wu, 2004; Cole and Fowler, 2006; Xiang et al., 2007; Zhang et al., 2010).

Pollen tubes are primarily divided into three regions: the apex, which is the growth region and denotes the hemisphere-shaped tip of the cell; the subapex, which is a transition region; and the shank, which is similar to other plant cells in that it contains the typical repertoire of plant organelles (Geitmann and Emons, 2000; Cai and Cresti, 2009). Accordingly, the actin filaments are also classified into three distinct structures in pollen tubes: longitudinal actin cables are observed in the shank, and dense actin structures are observed in the subapex and highly dynamic, but less abundant, actin filaments are observed in the extreme tip (Fu et al., 2001; Lovy-Wheeler et al., 2005; Cheung et al., 2008; Lee et al., 2008; Chen et al., 2009; Staiger et al., 2010; Su et al., 2012). These distinct actin structures are known to perform vital functions in pollen tube growth (Cole and Fowler, 2006; Ye et al., 2009). In particular, dense actin structures are believed to provide the molecular tracks necessary for the intracellular trafficking events required to support rapid tube extension (Lee and Yang, 2008; Yang, 2008; Cai and Cresti, 2009).

Actin binding proteins (ABPs) play crucial roles in modulating the organization and dynamics of actin filaments during pollen tube growth. Many ABPs have been identified as positive regulators of pollen tube growth by altering the stability and organization of actin filaments. For example, *Arabidopsis thaliana* FIMBRIN5 promotes pollen tube growth by its actin filament–bundling and –stabilizing activities to maintain the dynamic features of the actin cytoskeleton in the tube (Wu et al., 2010). *Arabidopsis VILLIN5* (*VLN5*) loss of function retards pollen tube growth by altering actin filament stability and turnover, suggesting a positive role for VLN5 in pollen tube growth (Zhang et al., 2010). However, genetic and cellular evidence currently fail to clearly demonstrate a role of ABPs in the negative control of

[1] These authors contributed equally to this work.
[2] Address correspondence to maotonglin@cau.edu.cn.
The author responsible for the distribution of materials integral to the findings presented in this article in accordance with the policy described in the Instructions for Authors (www.plantcell.org) is: Tonglin Mao (maotonglin@cau.edu.cn).
[W] Online version contains Web-only data.
www.plantcell.org/cgi/doi/10.1105/tpc.113.119768

pollen tube growth. Transient expression of lily (*Lilium longiflorum*) ACTIN BINDING PROTEIN29 (ABP29) results in actin filament fragmentation and inhibits pollen tube growth, indicating a negative role of ABP29 in pollen tube growth (Xiang et al., 2007). Identification of novel negative regulators of pollen tube growth would provide further insight into the molecular mechanisms underlying the regulation of pollen tube growth.

Recently, in vitro assays demonstrated that the activities of most ABPs are regulated by a variety of factors, such as Ca^{2+} and pH. *Arabidopsis* VLN5 exhibits diverse effects on the actin cytoskeleton in vitro, including barbed-end capping, filament bundling, and calcium-dependent severing (Zhang et al., 2010). Notably, a localized gradient of cytosolic free Ca^{2+} exists at the growing pollen tube apex (Qin and Yang, 2011). It is well accepted that the distribution of Ca^{2+} in the tip region overlaps with the actin filament gradient in pollen tubes (Fan et al., 2004). It is generally hypothesized that the Ca^{2+} gradient regulates the activities of Ca^{2+}-dependent ABPs, such as the villin/gelsolin/fragmin family. However, detailed analyses are required to determine the Ca^{2+}-related functions of ABPs on actin filaments and thereby on pollen tube growth.

Arabidopsis MDP25 was previously identified as a microtubule-destabilizing and calcium binding protein involved in hypocotyl cell elongation (Nagasaki et al., 2008; Li et al., 2011). MDP25 is localized to the plasma membrane and its function on cortical microtubules is regulated by the cytosolic calcium level (Li et al., 2011). In this study, we demonstrated that MDP25 is a novel ABP that negatively regulates pollen tube growth by modulating the actin cytoskeleton in the subapical region via its F-actin-severing activity.

RESULTS

MDP25 Is a Negative Regulator of Pollen Tube Growth

The data from the Affymetrix AG and ATH1 GeneChip arrays in the Genevestigator database (www.genevestigator.ethz.ch) indicate that *MDP25* is mostly expressed in flower tissues, especially in pollen, suggesting a potential role in pollen tube growth. To confirm this, we examined whether *MDP25* was expressed in the pollen and pollen tubes. Ten independent P_{MDP25}:β-glucuronidase (GUS) transgenic lines as described in a previous study (Li et al., 2011) were stained for GUS activity analysis. GUS staining revealed that *MDP25* was abundantly expressed in the pollen (Figure 1A) and the pollen tubes (Figure 1B).

We then examined whether the *MDP25* knockout mutant (*mdp25-1*) had phenotypes of aberrant pollen germination and pollen tube growth. Statistical analysis indicated that the germination rate of pollen from *mdp25-1* was not obviously different from that of wild-type Columbia-0 (Col-0) plants (Figure 1C). However, the pollen tube elongation of the *mdp25-1* mutant was enhanced. After 6 h of postgerminative growth in vitro, pollen tubes from *mdp25-1* were markedly longer than those of the wild-type Col-0 (Figures 1D to 1G). The length of *mdp25-1* pollen tubes was significantly longer than those of the wild type; whereas the average length of wild-type pollen tubes was 269.8 ± 46.7 μm ($n > 500$), it was 379.2 ± 37.37 μm for *mdp25-1* pollen tubes ($n > 500$) after 6 h of postgerminative growth. Furthermore, the growth rate of individual pollen tubes was measured using light microscopy (Figure 1H). The average growth rate of pollen tubes was calculated as being 73.8 ± 25.1 μm/h ($n = 47$) for the wild type and 96.7 ± 24 μm/h ($n = 57$) for *mdp25-1* after 3.5 h of postgerminative growth (Figure 1I). These results indicate that MDP25 has a negative effect on pollen tube growth in vitro.

The behavior of male gametophytes of the *mdp25-1* mutant was also observed. Wild-type stigmas were pollinated with wild-type and *mdp25-1* mutant pollen, respectively. By 4 h after pollination, more *mdp25-1* than wild-type pollen tubes had penetrated the style and reached the top of the transmitting tract (Figure 1J, a and b, arrows). At 8 h after pollination, wild-type pollen tubes were mostly growing in the transmitting tract (Figure 1J, c, arrow), while *mdp25-1* pollen tubes had almost reached the bottom of the transmitting tract (Figure 1J, d, arrow). Statistical analysis using paired Student's *t* tests indicated that the growth rate of pollen tubes from the *mdp25-1* mutants were significantly higher than that of the wild type (Figure 1K).

When a restricted amount of *mdp25-1* pollen grains were pollinated on wild-type stigmas, seed gaps and unfertilized ovules were detected. The proportion of seed setting was ~71%, while the proportion of seed setting was ~94% when pollinated with wild-type pollen grains on wild-type stigmas (Supplemental Figure 1A). Aniline blue staining showed that wild-type pollen tubes reached the majority of ovules (~85%), while a lower amount of *mdp25-1* pollen tubes reached the ovules (~61%) by 24 h after pollination, suggesting that the fast growth rate of *mdp25-1* pollen tubes disturbed the guidance of the tubes to the micropylar opening of the ovules (Supplemental Figure 1B). In addition, *mdp25-1* stigmas were pollinated with a limited amount of pollen grains from the wild-type or *mdp25-1* plants to test whether the female gametophytes of the *mdp25-1* mutant affected fertility. The seed gaps and unfertilized ovules were hardly detected when pollinated wild-type pollen grains were placed on *mdp25-1* stigmas. The proportion of seed setting was ~91%, while the proportion of seed setting was ~70% when *mdp25-1* stigmas were pollinated with *mdp25-1* pollen (Supplemental Figure 1C). These results suggest that downregulation of *MDP25* expression does not affect the fertility of female gametophytes.

MDP25 Directly Binds to and Severs Actin Filaments in Vitro

As a previous study has shown that MDP25 is a microtubule-destabilizing protein (Li et al., 2011), we investigated whether abnormal pollen tube growth of the *mdp25-1* mutant was related to microtubules. The previous study demonstrated that two sites of MDP25 (Lys-7 and Lys-18) were crucial for MDP25 to destabilize microtubules (Li et al., 2011). Consequently, in this study, P_{MDP25}:MDP25 K7A and P_{MDP25}:MDP25 K18A constructs were generated to complement the longer pollen tube phenotype of the *mdp25-1* mutant. More than 30 transgenic lines of each construct were obtained and typical transgenic lines (lines 2 and 16) were used for further analysis. Genetic evidence showed that the longer pollen tube phenotype of the *mdp25-1* mutant could be complemented by P_{MDP25}:MDP25 K7A and K18A (Figures 2D, 2E, and 2I), demonstrating that the

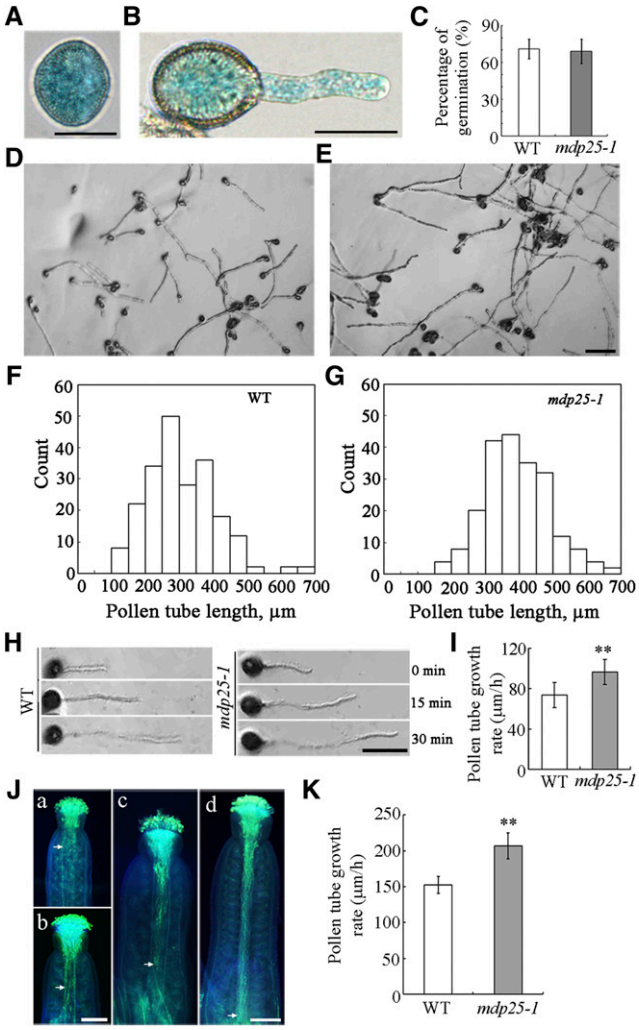

Figure 1. Pollen Tube Growth Is Promoted in the *MDP25* Loss-of-Function Mutant.

(A) and **(B)** Histochemical staining of GUS in the pollen grain and pollen tube of P_{MDP25}:GUS:T_{MDP25} transgenic plants. Bars = 20 μm.

(C) Graph of the pollen germination percentage at 6 h. Error bars represent mean ± SE (n > 500).

(D) and **(E)** Micrographs were taken of pollen tubes after germination for 6 h in vitro. Pollen was isolated from the wild type **(D)** and *mdp25-1* mutant **(E)**. Bar = 100 μm.

(F) and **(G)** Length distribution of pollen tubes: the wild type **(F)** and *mdp25-1* mutant **(G)**.

(H) Pollen tube growth rate was measured by tracking individual pollen tubes at 0, 15, and 30 min after germination for 3 h. Bar = 25 μm.

(I) Growth rates of wild-type and *mdp25-1* pollen tubes 30 min after a 3-h period (Student's t test, **P < 0.01). Error bars represent mean ± SE (n > 47).

(J) Pollen grains from wild-type Col-0 and *mdp25-1* mutants were used to pollinate wild-type stigmas. Pollen tubes were visualized by aniline blue staining. **(a)** and **(c)** Wild-type (Col-0) pollen grains germinated for 4 and 8 h, respectively. **(b)** and **(d)** Pollen grains from pollen of the *mdp25-1* mutant germinated for 4 and 8 h, respectively. The arrow indicates the position reached by most pollen tubes. Bars = 200 μm.

microtubule-destabilizing activity of MDP25 is not responsible for pollen tube growth inhibition.

Many ABPs modulate the organization and dynamics of actin filaments during pollen tube growth. Several ABPs bind to both microtubules and actin filaments, such as SB401, MAP18, and At-FH4 (Huang et al., 2007; Deeks et al., 2010; Zhu et al., 2013). To test if MDP25 binds to actin filaments, a high-speed cosedimentation assay was performed. As MDP25 is a calcium binding protein (Nagasaki et al., 2008), this assay was performed in the presence or absence of Ca^{2+} as previously described by Xiang et al. (2007). As shown in Figure 3A, a significant amount of MDP25 sediment was associated with F-actin following centrifugation at 100,000*g* with or without Ca^{2+} (Figure 3A, lanes 3 to 10). Gel density scanning analysis showed no obvious difference in the amount of MDP25 in the pellets between 10 μM Ca^{2+} or 1 mM EGTA (Figure 3B), indicating that MDP25 directly binds to F-actin with or without Ca^{2+}. To further confirm the ability of this protein to bind to actin filaments, in vitro immunofluorescence labeling was performed with an anti-glutathione *S*-transferase (GST) antibody. MDP25 was distributed specifically along actin filaments, exhibiting a dot-like structure (Supplemental Figures 2A to 2C). No staining was detected when using denatured GST-MDP25 or when the primary antibody was omitted (Supplemental Figures 2D to 2I), demonstrating that MDP25 binds to F-actin in vitro.

In addition, an increase in the amount of G-actin in the supernatant was detected in the presence of MDP25 with Ca^{2+}. When 5 μM preformed F-actin was incubated in the presence of 2, 4, or 6 μM MDP25 plus 10 μM Ca^{2+}, the percentage of actin in the supernatant was 17.25% ± 2.75%, 24.15% ± 2.45%, and 29.85% ± 3.25% (n = 3), respectively. This was significantly higher than the amount of actin in the supernatant without MDP25 (4.55% ± 1.78%, n = 3). Interestingly, the amount of actin in the supernatant was not significantly different (<8%, n = 3) when Ca^{2+} was chelated by EGTA (Figures 3A and 3C), suggesting that MDP25 severs or depolymerizes actin filaments in the presence of Ca^{2+}.

To further test this possibility, actin filaments were visualized by Alexa 488-phalloidin staining after incubation with 1 μM MDP25 in the presence or absence of Ca^{2+}. Analysis by confocal microscopy showed that more fragmented actin filaments were observed in the presence of MDP25 than in the absence of MDP25 (Figures 3D and 3E). Interestingly, F-actin was longer in the absence of MDP25 (>75% of filaments were longer than 10 μm, and <3% were shorter than 2 μm), whereas F-actin was shorter in the presence of MDP25 (<27% of filaments were longer than 10 μm, and ~14% were shorter than 2 μm) (Figure 3J). Notably, actin filaments were significantly fragmented when 10 μM Ca^{2+} was added in the presence of MDP25. With the addition of 10 μM Ca^{2+}, >44% of filaments were shorter than 2 μm, while the proportion of F-actin longer than 10 μm in length was reduced to 14% (Figures 3F and 3J). Fragmentation of F-actin was not observed when MDP25 was replaced with GST

(K) Graph of pollen tube growth rates of the wild type and *mdp25-1* mutant between 4 and 8 h after germination in vivo (Student's t test, **P < 0.01). Error bars represent mean ± SD (n > 200).

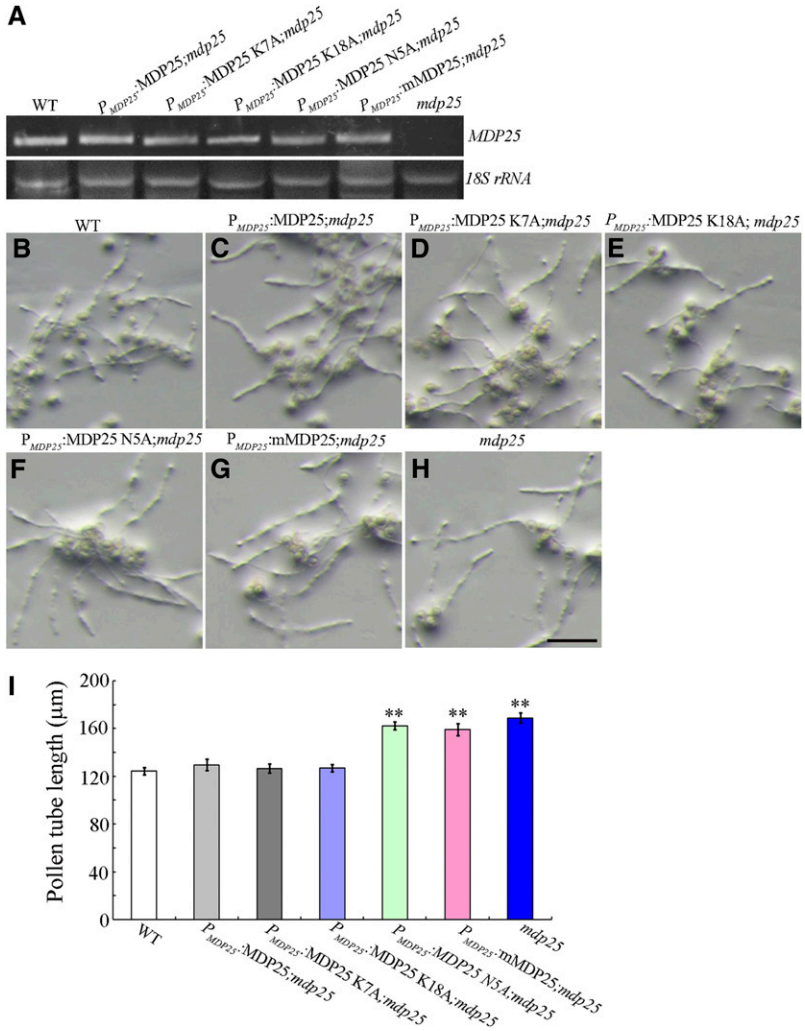

Figure 2. Complementation Assay of P_{MDP25}:MDP25, P_{MDP25}:MDP25 K7A, P_{MDP25}:MDP25 K18A, P_{MDP25}:MDP25 N5A, and P_{MDP25}:mMDP25.

(A) RT-PCR analysis of *MDP25* and mutated *MDP25* transcripts in seedlings of wild-type Columbia ecotype (WT), P_{MDP25}:MDP25-GFP, P_{MDP25}:MDP25 K7A-GFP, P_{MDP25}:MDP25 K18A-GFP, P_{MDP25}:MDP25 N5A-GFP, P_{MDP25}:mMDP25-GFP, and *mdp25-1* lines.

(B) to **(H)** Wild-type pollen tubes after 4 h of postgerminative growth **(B)**, P_{MDP25}:MDP25-GFP transgenic **(C)**, P_{MDP25}:MDP25 K7A-GFP transgenic **(D)**, P_{MDP25}:MDP25 K18A-GFP transgenic **(E)**, P_{MDP25}:MDP25 N5A-GFP transgenic **(F)**, and P_{MDP25}:mMDP25-GFP transgenic **(G)** *Arabidopsis* plants in the *mdp25-1* mutant background, and the *mdp25-1* mutant **(H)**. Bar = 100 μm.

(I) Graph of pollen tube lengths from more than 500 pollen tubes for each line. Error bars represent mean ± SE (Student's *t* test, $^{**}P < 0.01$).

protein plus Ca^{2+}, with more than 68% of F-actin being longer than 10 μm (Figures 3G and 3J).

To confirm the role of Ca^{2+} in MDP25-mediated actin filament fragmentation activity, previously identified Ca^{2+} binding site in the amino acid sequence of MDP25 (Nagasaki et al., 2008) was mutated (Supplemental Figure 3A). A cosedimentation assay showed that this mutation did not affect the binding of MDP25 to actin filaments (Supplemental Figures 3B and 3C). Confocal microscopy analysis showed that the mutated MDP25 protein (mMDP25) exhibited similar F-actin severing activity as wild-type MDP25 without the addition of Ca^{2+} (Figures 3H and 3J). Actin filament fragmentation was dramatically decreased when actin filaments were incubated with 1 μM mMDP25 and 10 μM Ca^{2+}, with 18% of filaments being shorter than 2 μm in length (Figures 3I and 3J).

The F-actin prepared from rhodamine-labeled G-actin was imaged using total internal reflection fluorescence microscopy (TIRFM). This was performed to investigate if the fragmentation of F-actin in the presence of MDP25 was indeed caused by the F-actin-severing activity of MDP25. GST protein was used as a negative control. Over a 500-s time period, no actin filament severing was observed in the presence of 100 nM GST plus 10 μM Ca^{2+} (a total of 120 actin filaments from three independent experiments) (Figures 4A and 4D; Supplemental Movie 1). However, breaks in the actin filaments were observed in the presence of 100 nM MDP25 (a total of 60 actin filaments from three

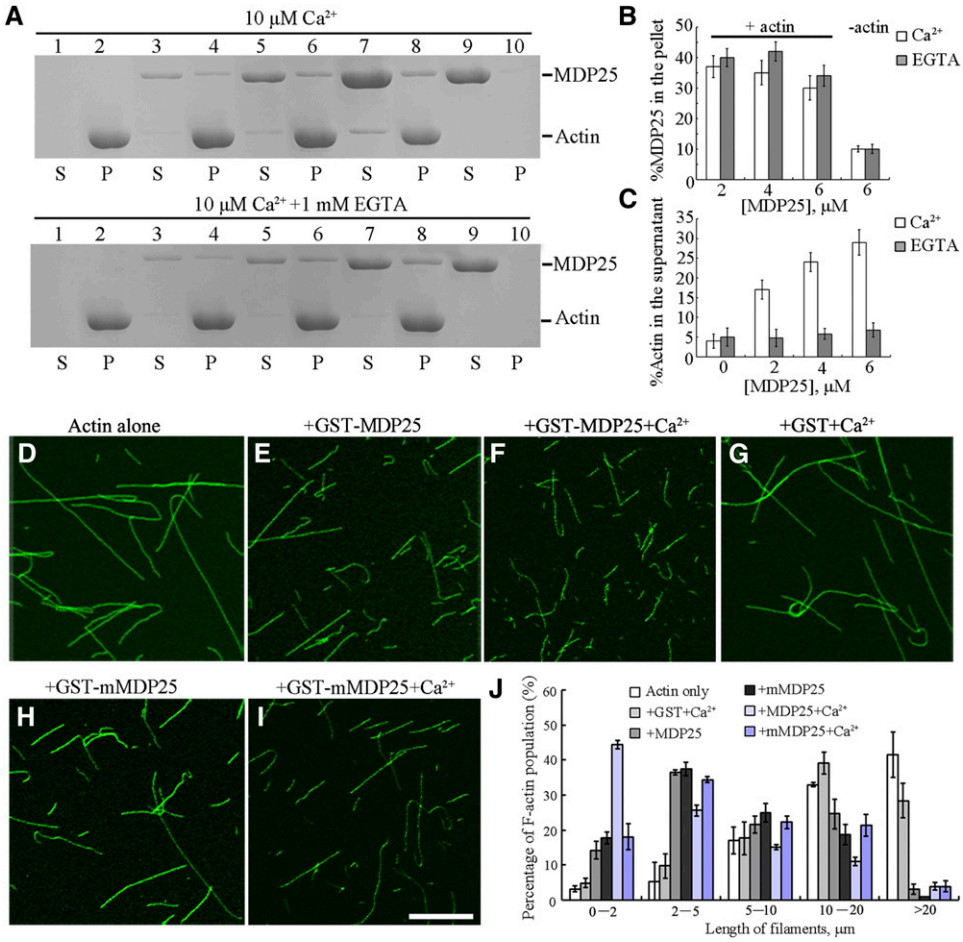

Figure 3. MDP25 Binds and Fragments Actin Filaments in Vitro.

(A) A high-speed cosedimentation assay was used to determine F-actin binding of MDP25. SDS-PAGE assay showed GST-MDP25 protein appeared mostly in the supernatant (S) in the absence of F-actin but cosedimented with F-actin in the pellets (P) in the presence of or absence of Ca^{2+}. Lanes 1 and 2, actin alone; lanes 3 and 4, actin in the presence of 2 μM MDP25; lanes 5 and 6, actin in the presence of 4 μM MDP25; lanes 7 and 8, actin in the presence of 6 μM MDP25; lanes 9 and 10, MDP25 alone. The top gel shows samples in the presence of 10 μM Ca^{2+}, and the bottom gel shows the samples in the presence of 1 mM EGTA.

(B) and **(C)** Statistical analysis for **(A)**.The amount of MDP25 and actin in the pellets and in the supernatant was estimated by gel density scanning and is expressed as a percentage of total MDP25 and actin, respectively. Error bars represent mean ± SD (n = 3).

(D) to **(I)** MDP25 fragments actin filaments. Actin filaments were visualized by the addition of 1 μM Alexa488-phalloidin. Preformed F-actin was incubated with 0 μM MDP25 **(D)**, 1 μM GST-MDP25 **(E)**, 1 μM GST-MDP25 plus 10 μM Ca^{2+} **(F)**, 1 μM GST plus 10 μM Ca^{2+} **(G)**, 1 μM GST-mMDP25 **(H)**, and 1 μM GST-mMDP25 plus 10 μM Ca^{2+} **(I)**. Bar = 10 μm.

(J) The length of F-actin was measured after incubation with or without MDP25 or mutated proteins in the presence and absence of Ca^{2+}. Error bars represent mean ± SE (n = 3).

independent experiments), indicating the occurrence of severing events with the addition of MDP25 (Figures 4B and 4D; Supplemental Movie 2). The addition of 100 nM MDP25 plus 10 μM Ca^{2+} further increased severing events, and the progressive shortening of actin filaments was more predominant, as revealed by quantified kinetics analysis (a total of 120 actin filaments from three independent experiments) (Figures 4C and 4D; Supplemental Movie 3). VLN2, which has F-actin-severing activity that is dependent on the presence of Ca^{2+} (Bao et al., 2012), was used as a positive control. When 1 nM VLN2 plus Ca^{2+} was added to actin filaments, severing events were significantly increased (Figure 4D; Supplemental Movie 4). To further characterize the severing activity of MDP25, severing frequency, as defined by the number of breaks per unit of filament length per second (breaks/μm/s) (Zhang et al., 2010; Bao et al., 2012), was analyzed (Figure 4E). The addition of MDP25 clearly increased severing frequency from 0.00005 ± 0.00014 (n = 30) to 0.00042 ± 0.00056 (n = 25) compared with the addition of GST protein plus Ca^{2+} (Student's t test, $P < 0.01$). Severing frequency was significantly increased to 0.00167 ± 0.00044 (n = 25) in the presence of MDP25 plus Ca^{2+}, which was lower than that observed with the addition of VLN2 plus Ca^{2+} (0.00349 ± 0.00098, n = 25) (Student's t test, $P < 0.01$). These

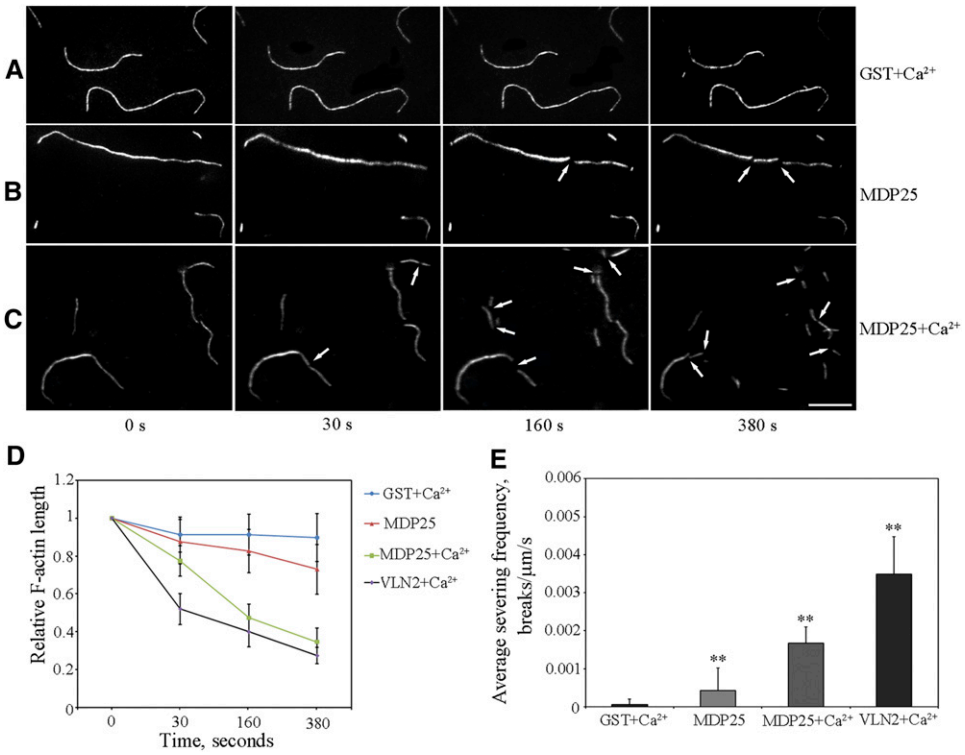

Figure 4. MDP25 Severs Actin Filaments in Vitro.

(A) to **(C)** Time series of prepolymerized rhodamine-labeled actin filaments. Over a 380-s time period, actin filaments were cut into fragments after introduction of 100 nM GST-MDP25 **(B)** (see Supplemental Movie 2 for the entire series). More intense severing activity of MDP25 was observed when 10 μM Ca^{2+} was added together with MDP25 **(C)** (see Supplemental Movie 3 for the entire series); severing events increased and the actin filament fragments were much shorter. Actin filaments were rarely changed when 100 nM GST plus 10 μM Ca^{2+} was introduced **(A)** (see Supplemental Movie 1 for the entire series) (arrow indicates where severing occurred). Bar = 10 μm.

(D) Quantitative kinetics indicated the progressive shortening of actin filaments. More than 60 prepolymerized rhodamine-labeled actin filaments of each sample were traced in the presence of 100 nM GST plus 10 μM Ca^{2+}, 100 nM GST-MDP25, 100 nM GST-MDP25 plus 10 μM Ca^{2+}, or 1 nM VLN2 plus 10 μM Ca^{2+}, respectively. Relative actin filament lengths were normalized to the initial length of the actin filaments at each time point. Data were collected from three independent experiments. Error bars indicate mean ± SD.

(E) Mean severing frequency calculated when rhodamine-actin filaments were incubated with 100 nM GST plus 10 μM Ca^{2+} or 100 nM GST-MDP25 and 100 nM GST-MDP25 plus 10 μM Ca^{2+}, respectively. A mean severing frequency of 1 nM VLN2 plus 10 μM Ca^{2+} was used as a positive control. Experiments were repeated three times. Each experiment examined more than 18 filaments. Results are presented as mean ± SE. **$P < 0.01$ compared with 100 nM GST plus Ca^{2+} by the Student's *t* test.

results indicate that MDP25 is capable of severing actin filaments and that this activity is significantly enhanced by Ca^{2+} in vitro.

Subcellular Localization of MDP25 in the Pollen Tube

MDP25 is reportedly located predominantly in the plasma membrane as determined by *N*-myristoylation. MDP25 has also been reported in the cytosol, although levels were low (Nagasaki et al., 2008). Treatment with the calcium-ionophore A23187 plus Ca^{2+} in vitro can induce disassociation of MDP25 from the plasma membrane into the cytosol (Li et al., 2011), suggesting that Ca^{2+} regulates MDP25 localization.

In this study, confocal microscopy showed that MDP25-GFP (for green fluorescent protein) was mainly localized in the plasma membrane at the shank region of the pollen tube but was absent in the membrane of the subapex and apex (Figures 5A, 5C, and 5D). Pollen tubes were then treated with 100 nM latrunculin B (LatB) for 5 min. LatB is a reagent that depolymerizes actin filaments (Wu et al., 2010). No difference in MDP25-GFP fluorescence signal in the plasma membrane was detected when the majority of actin filaments were disrupted in the pollen tube (Supplemental Figures 4A to 4C), suggesting that the targeting of MDP25 to the plasma membrane is independent to the presence of actin filaments.

As free Ca^{2+} forms a gradient at the growing pollen tube apex with high levels in the pollen tube tip, we hypothesized that the level of Ca^{2+} may affect the subcellular localization of MDP25 in the pollen tube. When the pollen tubes from MDP25-GFP transgenic plants were treated with 1 mM Ca^{2+} chelator 1,2-bis (2-aminophenoxy)ethane-*N*,*N*,*N*′,*N*′-tetraacetic acid tetrakis (acetoxymethyl ester) after 3 h of postgerminative growth, the MDP25-GFP appeared at the plasma membrane of the subapex

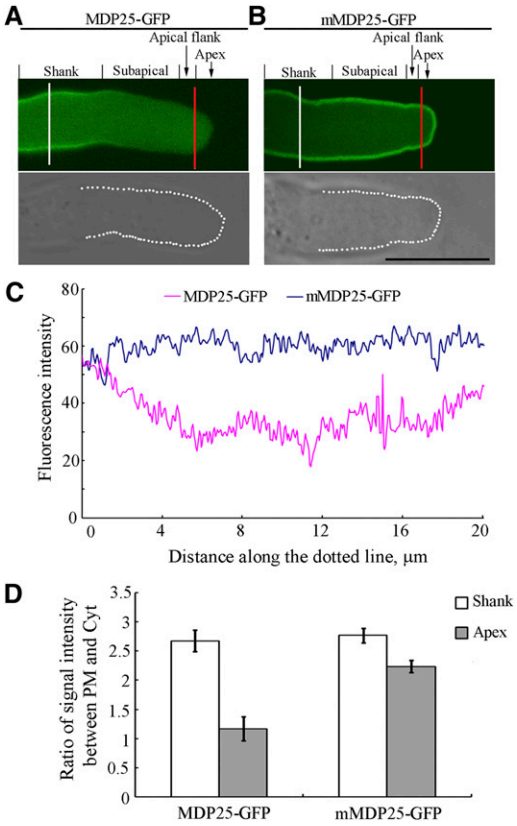

Figure 5. The Plasma Membrane Localization of MDP25-GFP Is Regulated by Ca^{2+} in the Pollen Tube.

(A) and **(B)** Mid-plane section of a MDP25-GFP pollen tube in which MDP25-GFP is mainly localized to the shank plasma membrane but not at the subapical region, the flank, or the apex **(A)**. Mid-plane section of an mMDP25-GFP pollen tube in which mMDP25-GFP is mainly localized to the plasma membrane at most pollen tube regions **(B)**. Bar = 10 μm. The bottom row of differential interference contrast images outlined with white dots (the bottom panels of **[A]** and **[B]**) in the mid-plane section displays the elevated fluorescence intensity in the surrounding plasma membrane as in **(C)**. The red and white lines indicate the position where arbitrary units were measured across the pollen tube shank and the tip **(D)**, respectively.

(C) Fluorescence intensities which tracked from top left to bottom left around the bottom row of images outlined with white dots in **(A)** and **(B)**.

(D) The ratio of fluorescence intensities between the plasma membrane with cytosol across the pollen tube shanks (white line) or across the pollen tube subapical region (red line) in **(A)** and **(B)**. Fluorescence intensity was measured across the lines with Image J 1.47 software (http://rsbweb.nih.gov/ij/; accessed August 7, 2013), and readings were then divided by the length of the line. More than 16 growing pollen tubes for each line were quantified. Error bars represent mean ± SD.

and in the apex (Supplemental Figures 5A to 5D). To further investigate how this subcellular distribution is affected by cytosolic Ca^{2+}, mMDP25-GFP was stably expressed in *Arabidopsis*. A fluorescence microscopy assay showed that mMDP25-GFP is predominantly localized to the plasma membrane along the whole length of the pollen tube (Figures 5B to 5D), demonstrating that the disassociation of MDP25 from the plasma membrane is mediated by Ca^{2+} in the subapical and apex regions of pollen tubes.

MDP25 Regulates the Actin Cytoskeleton in the Subapical Region of Pollen Tubes by Destabilizing Actin Filaments

To determine if the F-actin-severing activity of MDP25 plays a role in the organization and dynamics of actin filaments in pollen tubes, we observed the actin cytoskeleton. To visualize actin organization and dynamic features in pollen tubes, we used an actin filament marker *lifeact-mEGFP*, which is driven by the pollen-specific promoter *Lat52*. The *mdp25-1* mutant was crossed with the *lifeact-mEGFP* transgenic plant. Twenty-five lines of *mdp25-1;lifeact-mEGFP* were obtained and found to exhibit the longer pollen tube phenotype. Line 2, which exhibited the typical longer pollen tube phenotype, was selected for further analysis. Actin filaments in the shank and the subapical regions of the *mdp25-1* mutant and wild-type pollen tubes were observed by spinning disk microscopy. Thick, predominantly longitudinal actin filament bundles were observed in the shank of both the *mdp25-1* mutant and the wild-type pollen tubes. The thick actin filament bundles were absent at the subapical region of wild-type pollen tubes; however, they were relatively abundant in the pollen tubes of the *mdp25-1* mutant (Figure 6A; Supplemental Figure 6 and Supplemental Movies 5 and 6).

To quantify the extent of actin filament bundling and density in pollen tubes, skewness and occupancy were measured as previously described by Higaki et al. (2010). More actin bundles existed in the *mdp25-1* pollen tube subapical domes, as indicated by the dramatic increase of the mean skewness, compared with that of wild-type pollen tubes. However, actin filament bundling in the shank region of the *mdp25-1* pollen tube was similar to that in wild-type tubes (Figure 6B). The density of actin filaments in the *mdp25-1* pollen tube subapical region was higher than that in the wild-type pollen tubes, as indicated by the increase in the occupancy (i.e., density) of actin filaments in *mdp25-1* pollen tubes. There was no difference in the density of actin filaments in the shank region between the *mdp25-1* mutant and the wild-type pollen tubes. However, the density of actin filaments in the *mdp25-1* pollen tube apical region was decreased compared with that in the apical region of wild-type pollen tubes (Figure 6C). In conjunction, these measurements indicate that actin filament bundling and density were increased in the subapical region of *mdp25-1* pollen tubes, suggesting that MDP25 may have a destabilizing effect on actin filaments in the subapical region of pollen tubes.

To further test the effect of MDP25 on actin filaments, pollen tubes from the wild type and *mdp25-1* mutants that had undergone 3 h of postgerminative growth were cultured on medium containing increasing concentrations of LatB (0, 1, 2, 4, and 8 nM). The growth rate of pollen tubes was measured after treatment for 30 min. When cultured in the presence of LatB, the relative elongation rate of pollen tubes was lower in the wild type than in the *mdp25-1* mutant (Figure 6D). The effect of all concentrations of LatB was consistently more pronounced in the wild type than in the *mdp25-1* mutant. These observations indicate that actin filaments are less sensitive to LatB treatment in

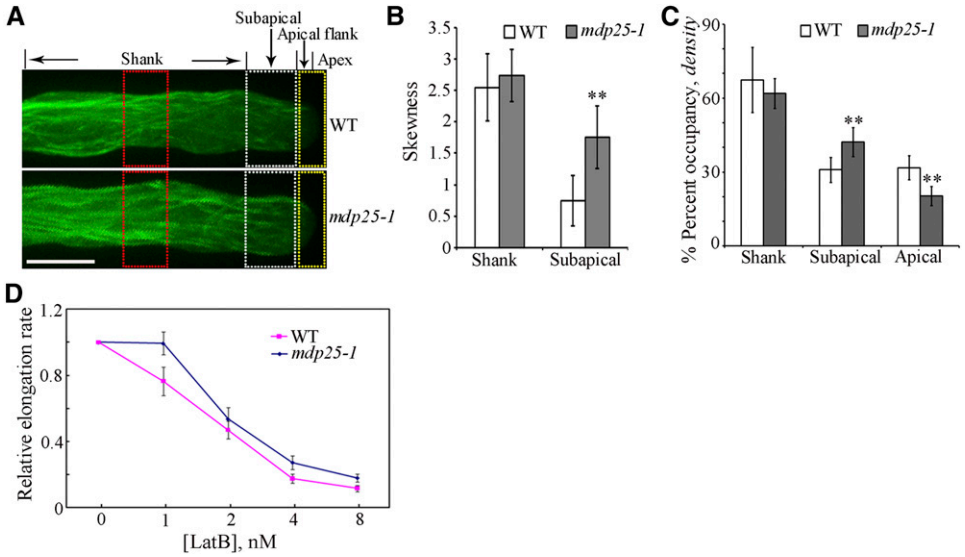

Figure 6. Characteristics of Actin Filaments Are Altered in the Subapical Region of Pollen Tubes of the *mdp25-1* Mutant.

Actin filaments were visualized in the pollen tube using lifeact-mEGFP driven by the pollen-specific promoter *Lat52*.

(A) The organization and density of actin filaments were altered in the apical region, while there was no obvious difference in the shank region of the *mdp25-1* and wild-type pollen tubes. The regions outlined with white, red, and yellow dots indicate the positions where arbitrary units were measured across the pollen tube in **(B)** and **(C)**, respectively. Bar = 10 μm.

(B) Bundling (skewness) analysis shown in **(A)** reveals increased actin filament bundling in the subapical region but not in the shank of the *mdp25-1* mutant compared with the wild type (Student's *t* test, **P < 0.01). More than 13 growing pollen tubes for each line were quantified. Error bars represent mean ± SE.

(C) Density (occupancy) analysis shown in **(A)** reveals increased actin filament density in the subapical region but decreased actin filament density in the apical region of the *mdp25-1* pollen tube compared with the wild-type pollen tube (Student's *t* test, **P < 0.01). The density of actin filaments was similar in the shank region between the *mdp25-1* and wild-type pollen tubes. More than 18 growing pollen tubes for each line were quantified. Error bars represent mean ± SE.

(D) The relative growth rate of more than 40 pollen tubes from the wild type and *mdp25-1* mutant of each treatment were measured in the presence of various concentrations of LatB. Error bars represent mean ± SE.

mdp25-1 pollen tubes. Confocal microscopy analysis revealed that subcellular localization of MDP25-GFP was not significantly altered in the treated pollen tubes, while the density of actin filaments in the subapical region decreased following a 30-min treatment with 8 nM LatB (Supplemental Figures 7A to 7D).

Actin dynamics were measured and the parameters associated with actin filament dynamics within the subapical dome were analyzed. Time-lapse images of actin filaments within the subapical region were visualized with an Andor iXon charge-coupled device camera. While severing events could be detected in wild-type pollen tubes (Figure 7A; Supplemental Movie 7), severing events were rarely detected in *mdp25-1* pollen tubes (Figure 7B; Supplemental Movie 8). The lifetime, elongation rate, and depolymerization rate of actin filaments in the *mdp25-1* subapical region were not significantly different from that in wild-type pollen tubes. However, the frequency of actin filament severing was significantly decreased in the *mdp25-1* subapical region compared with that in the wild-type tubes (Table 1). In particular, the severing frequency of actin filaments forming wide angles (>60°C) with the growth axis in the subapical region of *mdp25-1* pollen tubes (0.0053 ± 0.0013 break/μm/s, n = 31) was lower than that in the wild-type pollen tubes (0.0083 ± 0.0024 break/μm/s, n = 36). The maximal filament length of actin filaments was significantly increased in the *mdp25-1* pollen tubes compared with the wild-type pollen tubes. These results suggest that MDP25 plays a role in severing actin filaments in the subapical dome, thus modulating pollen tube growth.

Sequences That Target MDP25 to Actin Filaments and Microtubules Differ

Residues 1 to 23 of the N terminus of MDP25 were identified as being responsible for MDP25 targeting to microtubules and to the cellular membrane (Kato et al., 2010; Li et al., 2011). To investigate the potential role of these residues in regulating the actin cytoskeleton, we performed deletion analyses. Cosedimentation analyses showed that the truncated protein MDP25 24–225 did not bind to F-actin in vitro (Figure 8A). The ability of MDP25 to sever actin filaments via binding of MDP25 to phosphatidylinositol phosphates (PtdInsPs) in vitro (Nagasaki et al., 2008) was investigated. Preformed F-actin (1 μM) was incubated with 1 μM MDP25 preincubated with 0, 10, and 100 nM phosphatidylinositol 3,4,5-bisphosphate [PtdIns(3,4,5)P_3] and then visualized by Alexa 488-phalloidin staining. The confocal microscopy assay showed that an increasing amount of fragmented actin filaments were produced in the presence of

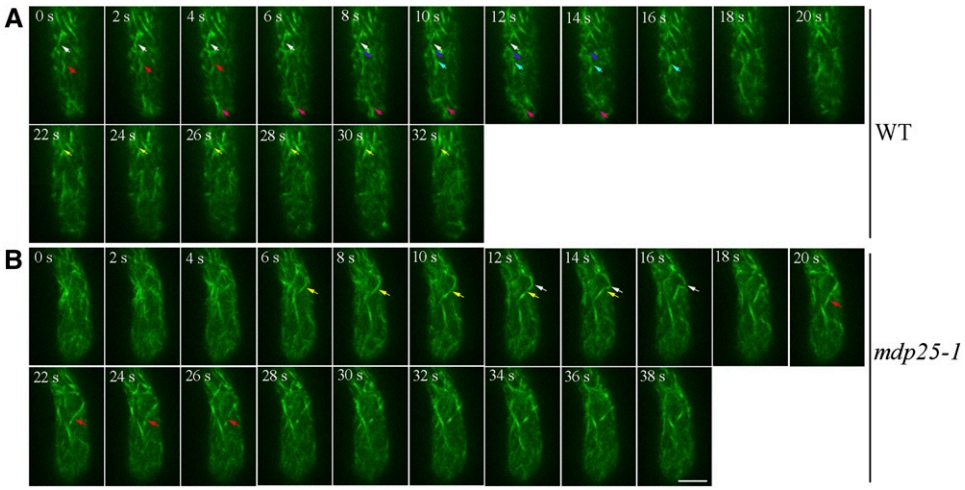

Figure 7. Actin Filament–Severing Frequency Is Decreased in the Subapical Region of *mdp25-1* Pollen Tubes.

Actin filaments were visualized in the pollen tube using lifeact-mEGFP driven by the pollen-specific promoter *Lat52*. The arrows indicate filament-severing events. Bar = 10 μm. See Supplemental Movies 7 and 8 for the entire series.

(A) Time-lapse images of actin filaments in the medial section of the subapical dome of a wild-type pollen tube. The arrows indicate filament-severing events. The different severing events are represented by arrows of different color.

(B) Time-lapse images of actin filaments in the medial section of the subapical dome of an *mdp25-1* pollen tube.

MDP25 alone (Figures 8B, a and b, and 8C). However, the amount of fragmented actin filaments was significantly decreased when incubated with MDP25 plus 10 and 100 nM PtdIns(3,4,5)P_3, respectively (Figures 8B, c and d, and 8C), demonstrating that the filament-severing activity of MDP25 is inhibited by binding to PtdInsPs in vitro.

Next, we attempted to identify the key site in residues 1 to 23 of the N terminus of MDP25. As previous studies have shown that two sites of MDP25 (Lys-7 and Lys-18) are crucial for MDP25 targeting and destabilization of microtubules (Li et al., 2011), we investigated if these sites were also important for MDP25 severing of actin filaments. Cosedimentation assays showed that MDP25 K7A and MDP25 K18A exhibited similar actin filament binding activity as wild-type MDP25 (Supplemental Figures 8A and 8B). Following this, 1 μM preformed F-actin was incubated with 1 μM either MDP25, MDP25 K7A, or MDP25 K18A for 30 min in the presence 10 μM $Ca^{2+}$and then visualized by Alexa 488-phalloidin staining. Confocal microscopy analysis showed that a significant amount of fragmented actin filaments were produced in the presence of the two mutated MDP25 proteins (MDP25 K7A and MDP25 K18A) with the addition of Ca^{2+}, which is similar to wild-type MDP25 (Figures 8D to 8G). This demonstrates that MDP25 K7A and MDP25 K18A lost their microtubule-destabilizing activity, while their actin filament–severing activity remained. The Asn residue of the MDP25 1–23 residues was then further mutated into Ala to investigate the effect of MDP25 N5A on actin filaments. A cosedimentation assay showed that the actin filament binding activity of MDP25 N5A was significantly decreased. When F-actin was incubated with 3 μM MDP25 or MDP25 N5A, the percentage of MDP25 N5A in the pellet was 14.15% ± 2.65% (n = 3), which is lower than that of wild-type MDP25 (38.65% ± 4.28%, n = 3) (Figures 8J and 8K). Furthermore, a confocal microscopy assay showed that, compared with wild-type MDP25, the actin filament–severing activity of MDP25 N5A was dramatically decreased with the addition of 10 μM Ca^{2+} (Figures 8H and 8I). In particular, >39% of F-actin was shorter than 2 μm, while the proportion of F-actin longer than 10 μm was reduced to 15% when treated with 1 μM wild-type MDP25 for 30 min. By contrast, less than 1.8% of F-actin was shorter than 2 μm and >69% longer than 10 μm when treated with 3 μM MDP25 N5A protein for 30 min (Figure 8I). In addition, similar to wild-type MDP25, MDP25 N5A also exhibited high microtubule destabilization activity (Supplemental Figures 9A to 9D), demonstrating that MDP25 N5A maintained normal function on microtubules but lost its actin filament-targeting activity. Confocal microscopy analysis revealed that the subcellular localization of MDP25 N5A in the pollen tube was similar to wild-type MDP25 (Supplemental Figures 4D and 4E). These results are consistent with the aforementioned hypothesis that targeting of MDP25 to the plasma membrane may not be related to the actin filaments.

Table 1. Actin Filament Dynamic Parameters in Wild type and *mdp25-1* Mutant

Dynamic Parameters	The Wild Type	*mdp25-1*
Lifetime (s)	20.4 ± 9.0 (45)	21.5 ± 12.3 (52)ND
Severing frequency (break/μm/s)	0.031 ± 0.002 (54)	0.015 ± 0.002 (62)**
Max. filament length (μm)	17.0 ± 1.6 (60)	21.8 ± 8.4 (60)*
Elongation rate (μm/s)	0.66 ± 0.33 (38)	0.72 ± 0.12 (35)ND
Depolymerization rate (μm/s)	0.52 ± 0.12 (38)	0.55 ± 0.23 (36)ND

The parameters that associated with single actin filament dynamics in wild-type and *mdp25-1* pollen tubes were quantified from spinning disk confocal micrographs. Quantification of *P < 0.05 and **P < 0.01; ND, no significant difference by a Student's *t* test. The values are expressed as the mean ± SD.

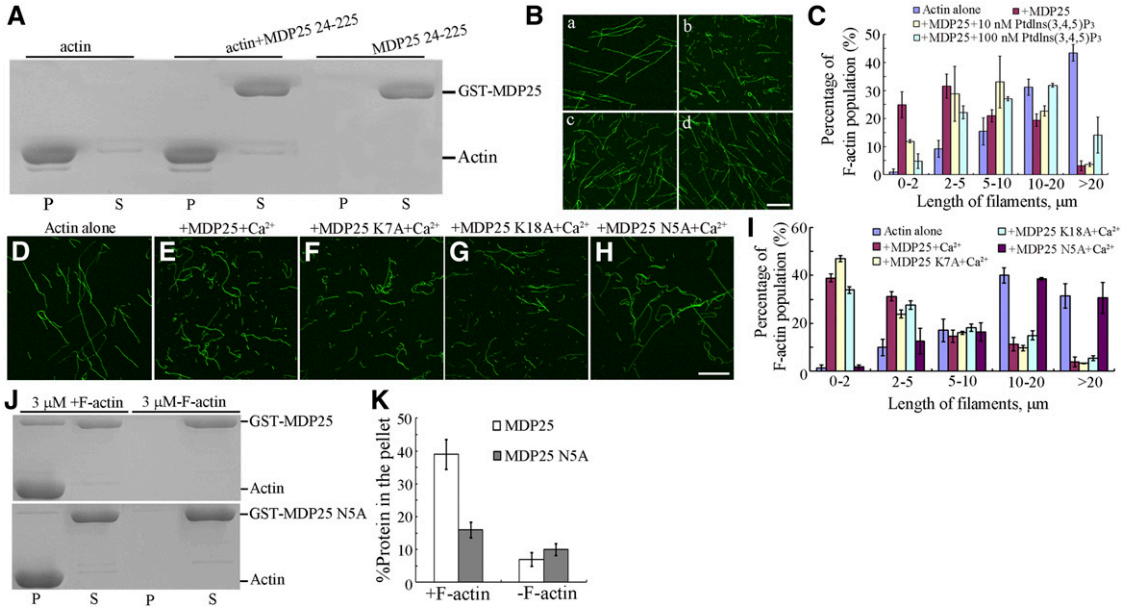

Figure 8. Residues 1 to 23 of MDP25 Are Essential for Targeting MDP25 to Actin Filaments.

(A) MDP25 24-225 did not cosediment with actin filaments.
(B) The actin-filament-severing activity of MDP25 was dramatically decreased when binding to PtdIns(3,4,5)P_3 in vitro. Preformed F-actin was incubated with 0 μM MDP25 **(a)**, 1 μM GST-MDP25 **(b)**, 1 μM GST-MDP25 preincubated with 10 nM PtdIns(3,4,5)P_3 **(c)**, and 1 μM GST-MDP25 preincubated with 100 nM PtdIns(3,4,5)P_3 **(d)**.
(C) Percentage of F-actin population of different actin filament length **(B)**. Error bars represent mean ± SE (n = 3).
(D) to **(H)** Actin filament-fragmented activity of MDP25 N5A was dramatically decreased. Preformed F-actin was incubated with 0 μM MDP25 **(D)**, 1 μM GST-MDP25 plus 10 μM Ca^{2+} **(E)**, 1 μM GST-MDP25 K7A plus 10 μM Ca^{2+} **(F)**, 1 μM GST-MDP25 K18A plus 10 μM Ca^{2+} **(G)**, and 3 μM GST-MDP25 N5A plus 10 μM Ca^{2+} **(H)**. Actin filaments were visualized by the addition of 1 μM Alexa 488-phalloidin. Bar = 10 μm.
(I) Graph of percentage of F-actin population of different actin filament length. Error bars represent mean ± SE (n = 3). Mutated MDP25 N5A affected MDP25 targeting to F-actin.
(J) Compared with wild-type MDP25, the activity of MDP25 N5A targeting to actin filaments was decreased. S, supernatant; P, pellet.
(K) The results of the quantitative analysis of the amount of wild-type MDP25 and MDP25 N5A protein in the pellets. The amount of protein was determined by gel scanning from three independent experiments. Error bars represent mean ± SD.

MDP25 Modulates Pollen Tube Growth in an Actin Filament– and Calcium-Dependent Manner

The above-mentioned results show that the microtubule-destabilizing activity of MDP25 is not involved in the negative regulation of pollen tube growth by MDP25. We then went on to investigate whether the actin filament–severing and calcium binding activities of MDP25 are related to its modulation of pollen tube growth. Constructs were generated to complement the longer pollen tube phenotype of *mdp25-1*. P_{MDP25}:MDP25 (wild-type MDP25), P_{MDP25}:mMDP25 (mutated calcium binding sites), and P_{MDP25}:MDP25 N5A (mutated actin filament–severing site) with a GFP tag at the C terminus were constructed and introduced into the *mdp25-1* mutant by *Agrobacterium tumefaciens*–mediated transformation. More than 15 lines in each transgenic background were obtained and representative transgenic lines were used for further analysis.

RT-PCR analysis showed that the mRNA level of *MDP25* or *MDP25* mutants in the transgenic lines was similar to that in the wild type (Figure 2A). The pollen tube elongation of each line was then assessed in vitro. The longer pollen tube phenotype of *mdp25-1* could be complemented by P_{MDP25}:MDP25-GFP (Figures 2B, 2C, and 2I), indicating that the MDP25-GFP protein was functional in vivo and that the aberrant pollen tube phenotype of *mdp25-1* was associated with *MDP25* expression level. However, P_{MDP25}:MDP25 N5A and P_{MDP25}:mMDP25 were not capable of complementing *mdp25-1* (Figures 2F to 2I), demonstrating that the calcium binding and actin filament–severing activities of MDP25 are both essential for correct pollen tube growth.

DISCUSSION

In this study, we characterized the function of *Arabidopsis* MDP25, revealing that MDP25 regulates pollen tube elongation by severing actin filaments in the subapical region.

Calcium Regulates the Actin Filament–Severing Activity of ABPs and thereby Exhibits Diverse Effects on Pollen Tube Growth

Pollen tube elongation exhibits a unique nonlinear pulse and sustained oscillation, which is simultaneously correlated with

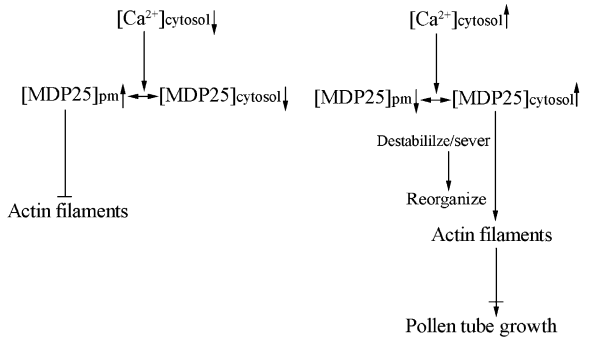

Figure 9. Model of MDP25 Function on Actin Filaments in the Mediation of Pollen Tube Growth.

In the shank region of the pollen tube, which is characterized by a resting state of cytosolic calcium level, MDP25 predominantly binds to the plasma membrane (pm) and its actin filament-targeting domain is covered with PtdInsPs. In the subapical region of the pollen tube, which is characterized by higher cytosolic calcium levels, induced MDP25 disassociation from the plasma membrane occurs. Cytosolic MDP25 destabilizes actin filaments by severing them, which alters the organization and density of actin filaments, further inhibiting pollen tube growth.

oscillatory changes of cytosolic Ca^{2+} concentration ($[Ca^{2+}]_c$) in the apical region of pollen tubes (Cheung and Wu, 2008; Yan et al., 2009). The Ca^{2+} signal is perceived by multiple components, including calmodulin and ABPs to further regulate pollen tube growth (Rato et al., 2004; Yokota et al., 2005; Gu et al., 2005; Wang et al., 2008; Chen et al., 2009). Many ABPs have been identified as being involved in the severing of actin filaments in the presence of Ca^{2+}, including MAP18, VLN5, ABP29, and MDP25. Decreased or increased expression of these ABPs results in diverse defective phenotypes of pollen tube growth and development. For example, decreasing or increasing the level of *MAP18* can induce abnormal directional pollen tube growth, yet does not affect pollen tube growth rate (Zhu et al., 2013). Decreasing *Arabidopsis VLN5* expression level inhibits pollen tube elongation, suggesting a positive role of VLN5 during pollen tube growth (Zhang et al., 2010). Increasing lily *ABP29* expression levels inhibits pollen tube elongation, while decreasing *MDP25* levels promotes pollen tube elongation, suggesting a negative role of ABP29 and MDP25 during pollen tube growth (Xiang et al., 2007; this study). It remains unknown how plants coordinate the actin filament–severing activity of these proteins in response to Ca^{2+} in the maintenance of a dynamic actin filament array to modulate pollen tube growth. Thus, multiple regulators of the actin cytoskeleton, such as F-actin-severing ABPs, that promote or inhibit pollen tube growth remain to be characterized.

Pollen tubes show a tip-focused $[Ca^{2+}]_c$ gradient (i.e., the concentration of Ca^{2+} gradually decreases to basal levels in the subapical region, 20 μm away from the extreme apex) (Pierson et al., 1996; Holdaway-Clarke et al., 1997). While low levels of MDP25 are detected in the cytosol, MDP25 is predominantly localized on the plasma membrane (Nagasaki et al., 2008; Kato et al., 2010). The N-terminal region of MDP25 (23 amino acid residues) binds to PtdInsPs when MDP25 is located on the plasma membrane (Kato et al., 2010). The biochemical assays performed in this study demonstrated that this region is also essential for targeting MDP25 to actin filaments. Furthermore, the actin filament–severing activity of MDP25 is significantly decreased in the presence of PtdIns(3,4,5)P_3, suggesting that, unlike the group I formin *Arabidopsis* FH4 (Deeks et al., 2010), MDP25 may not bind to actin filaments when located on the plasma membrane. Thus, the plasma membrane represents a pool that sequesters most of the MDP25 from actin filaments, thus inhibiting its actin filament–severing activity. However, cellular localization and point mutation analysis in this study showed that MDP25-GFP loses its membrane localization at the subapical region and apex flank, which may be largely due to the presence of Ca^{2+}. Such results demonstrate that physiological concentrations of Ca^{2+} at these regions are capable of regulating MDP25 translocation. This phenomenon has been shown in MDP25-GFP stably transgenic *Arabidopsis* suspension cells treated with the calcium-ionophore A23187 plus Ca^{2+} and in etiolated MDP25-GFP–overexpressing hypocotyl cells treated with light (Li et al., 2011), suggesting that cytosolic Ca^{2+} is a key regulator of the subcellular translocation and functions of MDP25. Thus, to obtain a comprehensive understanding of the involvement of actin filament–severing proteins in the regulation of pollen tube growth in response to Ca^{2+}, future studies are required to investigate their functions via multiple cellular, genetic, and physiological assays.

MDP25 Destabilizes Actin Filaments in the Subapical Region to Modulate Pollen Tube Growth

Regulation of pollen tube growth is crucial for delivering sperm for fertilization. It is well known that actin filaments form distinct arrays that mediate pollen tube growth, particularly at the subapical region (Cheung and Wu, 2008; Chen et al., 2009; Su et al., 2012). The mechanisms by which these dynamic actin structures are generated and maintained remain largely unknown. In this study, MDP25 was shown to localize to the cytosol in the subapical region, but in the plasma membrane in the shank (Figure 4), implying that MDP25 may be an important regulator of actin organization and dynamics in the subapical region of the pollen tube. Consistent with this hypothesis, the *MDP25* loss-of-function mutant exhibited significantly decreased F-actin-severing frequency, and pollen tubes of the *mdp25-1* mutant were less sensitive to LatB treatment, suggesting that MDP25 destabilizes actin filaments. Actin filaments are more sensitive to LatB treatment in the pollen tubes of *VLN5* loss-of-function mutants. In addition, downregulation of *VLN5* can lead to unstable actin filaments in the pollen tube, suggesting that VLN5 stabilizes actin filaments (Zhang et al., 2010; Qu et al., 2013). By contrast, overexpression of ABP29 resulted in actin patches or dispersion of short filament aggregates in the pollen tube, suggesting that ABP29 destabilizes actin filaments (Xiang et al., 2007). Consequently, ABPs may induce stabilization or destabilization of actin filaments, further promoting or inhibiting pollen tube growth. Future research is necessary to determine the detailed molecular mechanisms involved in this regulation.

Once pollen grains germinate and produce pollen tubes on the stigma of the pistil, pollen tubes grow rapidly and are guided to the micropylar opening of the ovules (Kägi and Gross-Hardt, 2007; Crawford and Yanofsky, 2008). Many positive regulators have been identified in this process, such as *Arabidopsis* cyclase-associated protein and FIMBRIN5 (Deeks et al., 2007; Wu et al., 2010). This study showed significant differences of seed settings when restricted *mdp25-1* pollen grains were pollinated on wild-type stigmas, suggesting that negative regulation of pollen tube growth is also necessary for fertilization.

Besides binding to actin filaments, MDP25 also destabilizes microtubules (Li et al., 2011). An increasing number of proteins that bind to both microtubules and actin filaments have been identified in plants, including SB401, a pollen-specific protein from *Solanum berthaultii*, and *Arabidopsis* FH4, which belongs to the group I formin family (Huang et al., 2007; Deeks et al., 2010). However, genetic and cellular evidence are currently lacking as to how these proteins perform their specific functions in various types of cells or in response to diverse physiological processes. In vitro biochemical assays have predominantly been used to distinguish the proteins' preferred activity on microtubules or actin filaments. In this study, we provide genetic evidence that MDP25 regulates pollen tube elongation by regulating actin filaments and not by its microtubule-destabilizing activity. Consequently, we propose the following model for the function of MDP25 on actin filaments in pollen tubes (Figure 9). The plasma membrane represents a pool that sequesters MDP25 from actin filaments to maintain F-actin stabilization in the shank region. MDP25 is disassociated into the cytosol in the subapical region due to the high concentration of Ca^{2+}. MDP25 in the cytosol then induces actin filament destabilization by severing actin filaments, which alters the organization and density of actin filaments with concomitant effects on pollen tube growth. Exactly how MDP25 physically binds to and regulates actin filaments in the pollen tube is the subject of future studies.

METHODS

Plant Materials and Growth Conditions

All plants and materials used in this study were from the Col-0 ecotype background. Seeds were sterilized and placed on Murashige and Skoog medium (Sigma-Aldrich) containing 1% agar and 3% Suc. Plants were grown in an air-conditioned growth room at 22°C under 16-h-light/8-h-dark cycles.

Pollen Germination and Pollen Tube Growth Measurement

In vitro pollen germination was performed as previously described by Ye et al. (2009). Flowers obtained from *Arabidopsis thaliana* plants 2 weeks after bolting were used to examine pollen tube phenotypes. Pollen was harvested from newly opened flowers and placed on pollen germination medium [1 mM $CaCl_2$, 1 mM $Ca(NO_3)_2$, 1 mM $MgSO_4$, 0.01% (w/v) H_3BO_3, and 18% (w/v) Suc solidified with 1% (w/v) agar, pH 7.0]. The plates were cultured at 28°C under high humidity. Percentage of germinated pollen grains was determined after 6 h. To determine the effects of LatB on pollen tubes, pollen tubes that had been incubated in germination medium for 3 h were treated with various concentrations of LatB in the liquid germination medium. Pollen growth rate was measured after treatment for 30 min by microscopy analysis.

Analysis of MDP25 Promoter:GUS Activity in Pollen Tubes

A DNA fragment of the MDP25 promoter containing 1011 bp upstream of the translation start site was amplified by PCR. The sequence was then cloned into the pCAMBIA1391 vector (Invitrogen). The resulting construct was then transformed into *Arabidopsis* plants using *Agrobacterium tumefaciens* (strain GV3101). The homozygous seedlings were used for histochemical localization of GUS activity in pollen grains or pollen tubes. The GUS staining procedure was performed as previously described by Sundaresan et al. (1995) and Yang et al. (1999).

F-Actin Binding Assay

Actin was purified as previously described (Spudich and Watt, 1971). High-speed cosedimentation experiments were performed according to Kovar et al. (2000). The purified proteins were centrifuged at 200,000*g* at 4°C for 20 min prior to use. Various concentrations of MDP25 were incubated with F-actin (polymerized from 5 μM G-actin) in KMEI buffer (50 mM KCl, 1 mM $MgCl_2$, 1 mM EGTA, and 10 mM imidazole-HCl, pH 7.0) in the presence or absence of Ca^{2+} for 2 h, followed by centrifugation at 4°C for 30 min at 100,000*g*. The supernatant and pellets were subjected to SDS-PAGE. The amount of fusion protein bound to the F-actin was determined by gel scanning, and the binding ratio was analyzed using the Alpha Image 2200 documentation and analysis system (Alpha Innotech).

Immunofluorescence staining experiments were performed to investigate the binding of MDP25 to actin filaments. Preformed F-actin was stabilized with Alexa 488-phalloidin (1:1) and was then incubated with GST-MDP25 at a molar ratio of 4:1 for 10 min at room temperature in KMEI buffer. The samples were labeled with anti-GST antibody at a 1:500 dilution for 15 min. The secondary antibody of tetramethylrhodamine-5(and 6-)-isothiocyanate–conjugated goat anti-mouse IgG (1:200 dilution) was added to the mixture for another 15 min. The samples were transferred onto slides coated with 0.1% (v/v) poly-L-Lys. Fluorescence images of actin filaments and GST-MDP25 were visualized using a Zeiss LSM 510 META confocal microscope with Zeiss ×63 oil objectives (Plan-Apochromat; numerical aperture of 1.4). The negative controls were incubated with denatured MDP25 or with secondary antibody alone.

Fluorescence Microscopy Assay

To visualize the effects of MDP25 on actin filaments, a fluorescence microscopy assay was performed. MDP25 or mutated fusion proteins at a concentration of 1 μM were incubated with 1 μM preformed F-actin in the presence or absence of 10 μM Ca^{2+} at room temperature for 30 min. Actin filaments were then labeled with an equimolar concentration of Alexa 488-phalloidin. Actin filaments were diluted to a final concentration of 10 nM in fluorescence buffer (10 mM imidazole, pH 7.0, 50 mM KCl, 2 mM $MgCl_2$, 1 mM EGTA, 100 mM DTT, 100 μg/mL Glc oxidase, 15 mg/mL Glc, 20 μg/mL catalase, and 0.5% methylcellulose) according to Huang et al. (2003). The diluted samples were fixed with 1% glutaraldehyde for observation by confocal microscopy.

To investigate the actin filament–severing activity of MDP25 when binding to PtdInsPs in vitro, PtdIns(3,4,5)P_3 (Echelon) was used (Nagasaki et al., 2008). MDP25 was preincubated with 0, 10, and 100 nM PtdIns(3,4,5)P_3 for 2 h at room temperature. Preformed F-actin (1 μM) was added to the reaction for another 30 min. The actin filaments were visualized by Alexa 488-phalloidin staining.

TIRFM Assay

Actin was labeled with 5- and 6-carboxytetramethylrhodamine succinimidyl ester–rhodamine as previously described (Blanchoin et al., 2000). TIRFM experiments were conducted according to Kovar and Pollard (2004). Rhodamine-labeled actin at a concentration of 4 μM was polymerized in

KMEI buffer for 1 h at room temperature. The flow cell was incubated with 100 nM *N*-ethylmaleimide myosin for 2 min and then equilibrated with 1% BSA. After washing with 1× TIRF buffer (10 mM imidazole, pH 7.0, 50 mM KCl, 1 mM $MgCl_2$, 1 mM EGTA, 50 mM DTT, 0.2 mM ATP, 50 μM $CaCl_2$, 15 mM Glc, 20 μg/mL catalase, 100 μg/mL Glc oxidase, 0.5% methylcellulose, and 0.2% BSA), polymerized F-actin (100 nM) was injected into the flow cell. Subsequently, 100 nM purified MDP25 was added into the flow cell. Images were acquired for a 500-s period. The time-lapse process was monitored using an Olympus IX81 microscope and a TIRF microscope (Andor Revolution XD) equipped with an Andor iXon charge-coupled device camera (Andor Technology) and a ×100 1.4–numerical aperture Olympus objective. TIRF illumination was performed at λ = 568 nm. The exposure time was 100 ms. Images were captured using Andor ImageQ software, version 1.1 (Andor Technology), and analyzed with Image J 1.47 software (http://rsbweb.nih.gov/ij/; accessed August 7, 2013).

P_{MDP25}:MDP25-GFP Construction and Expression in *Arabidopsis*

A fragment of 1011 bp upstream of the initiation codon (ATG) of *MDP25* to the stop codon (TGA) was amplified and reconstructed into a pCAMBIA1390 vector. GFP was amplified and ligated at the C terminus of *MDP25*. The constructs were transformed into *Arabidopsis* plants by *Agrobacterium* (strain GV3101). The homozygous lines were used for the subsequent complementation analyses.

Visualization and Quantification of Actin Filament Dynamics

Pollen tubes expressing *Lat52:lifeact-EGFP* were observed with an Andor iXon charge-coupled device camera. Time-lapse images were captured every 2 s. Parameters, including severing frequency, maximum filament length, elongation rate, depolymerization rate, and filament lifetime, were calculated as previously described in Image J software (Staiger et al., 2009; Henty et al., 2011). The filaments that could be tracked over four successive frames were used for the calculations. The severing frequency for each actin filament was calculated as the number of breaks, per unit filament length, per unit time. Maximum filament length was calculated as the longest length of a tracked filament during the time course. Maximum filament lifetime was calculated as the amount of time a filament was present, from initial filament origin until all pieces of the filament could no longer be tracked. Elongation rate was determined by filament length versus time with the data fitted with a linear function in Excel. To determine the depolymerization rate, a kymograph was prepared from growing actin filaments that were computationally straightened and plotted as filament length versus time in Image J software. Rates were estimated from the slope of a line placed on the kymograph at the presumed pointed end of the growing filament.

Quantitative Analyses of the Actin Filament Array in the Pollen Tube Subapical Region

Skewness was measured to quantify the extent of F-actin bundling and the percentage of occupancy of F-actin in pollen tubes was performed as previously described (Higaki et al., 2010; Li et al., 2012). Data were analyzed in Image J software (http://rsbweb.nih.gov/ij/; version 1.38).

RT-PCR Analysis of Transcript Levels

RT-PCR was performed to assess *MDP25* transcript levels in wild-type and transgenic seedlings. The PCR products were visualized by ethidium bromide staining on an agarose gel. Columbia ecotype seedlings or P_{MDP25}:MDP25-GFP, P_{MDP25}:MDP25 K7A-GFP, P_{MDP25}:MDP25 K18A-GFP, P_{MDP25}:MDP25 N5A-GFP, and P_{MDP25}:mMDP25-GFP transgenic homozygous seedlings grown for 7 d were used for the analysis. Total RNA was isolated using TRIzol reagent (Invitrogen). Primers used for RT-PCR were 5′-CGCAGGACCGGTCACGTTCA-3′ and 5′-TTCAGCCACTGGCGCTGTCG-3′. The *18S rRNA* was also amplified as a loading control using the primers 5′-CGGCTACCACATCCAAGGAA-3′ and 5′-GCTGGAATTACCGCGCGGCT-3′.

Accession Number

Sequence data described in this article can be found in the Arabidopsis Genome Initiative under the accession number At4g20260 (MDP25).

Supplemental Data

The following materials are available in the online version of this article.

Supplemental Figure 1. *MDP25* Loss-of-Function Mutant Affects Fertilization of Embryos and Pollen Tube Growth.

Supplemental Figure 2. MDP25 Colocalizes with F-Actin in Vitro.

Supplemental Figure 3. Mutated Calcium Binding Site of MDP25 Does Not Affect F-Actin Binding.

Supplemental Figure 4. Plasma Membrane Localization of MDP25 Is Independent of the Presence of Actin Filaments.

Supplemental Figure 5. Subcellular Localization of MDP25-GFP Is Affected When Tubes Are Treated with Ca^{2+} Chelator.

Supplemental Figure 6. Organization and Density of Actin Filaments Are Altered in the Subapical Region of Pollen Tubes of the *mdp25-1* Mutant.

Supplemental Figure 7. Subcellular Localization of MDP25-GFP in Pollen Tubes Is Not Altered by LatB Treatment.

Supplemental Figure 8. Mutation of Two Sites of MDP25 Does not Affect It Targeting to Actin Filament.

Supplemental Figure 9. MDP25 N5A Destabilizes Microtubules in Vitro.

Supplemental Movie 1. GST Protein Does Not Sever Actin Filaments.

Supplemental Movie 2. MDP25 Severs Actin Filaments.

Supplemental Movie 3. Ca^{2+} Dramatically Enhances the Actin Filament Severing Activity of MDP25.

Supplemental Movie 4. The Actin Filament–Severing Activity of VLN2.

Supplemental Movie 5. Actin Filaments in a Wild-Type Pollen Tube.

Supplemental Movie 6. Actin Filaments in a *mdp25-1* Pollen Tube.

Supplemental Movie 7. Medial Section Showing Actin Filament Dynamics in the Subapical Region of a Wild-Type Pollen Tube.

Supplemental Movie 8. Actin Filament Dynamics at the Medial Section of an *mdp25* -1 Mutant Pollen Tube.

ACKNOWLEDGMENTS

We thank Ming Yuan (China Agricultural University) for critical reading and comments on the article and Shanjin Huang (Chinese Academy of Sciences) for providing *Arabidopsis* seeds expressing *Lat52:lifeact-mEGFP* and for recombinant VLN2 protein. This research was supported by grants from the National Basic Research Program of China (2012CB114200 to T.M.), the Natural Science Foundation of China (31222007 and 31070258 to T.M.), and the Program for New Century Excellent Talents in University (NCET-12-0523 to T.M.).

AUTHOR CONTRIBUTIONS

T.M. designed the project. T.Q., X.L., J.L., J.S., and L.S. performed specific experiments and analyzed the data. T.M. supervised the project and wrote the article.

Received October 18, 2013; revised December 5, 2013; accepted December 19, 2013; published January 14, 2014.

REFERENCES

Bao, C., Wang, J., Zhang, R., Zhang, B., Zhang, H., Zhou, Y., and Huang, S. (2012). *Arabidopsis* VILLIN2 and VILLIN3 act redundantly in sclerenchyma development via bundling of actin filaments. Plant J. **71:** 962–975.

Blanchoin, L., Amann, K.J., Higgs, H.N., Marchand, J.B., Kaiser, D.A., and Pollard, T.D. (2000). Direct observation of dendritic actin filament networks nucleated by Arp2/3 complex and WASP/Scar proteins. Nature **404:** 1007–1011.

Boisson-Dernier, A., Roy, S., Kritsas, K., Grobei, M.A., Jaciubek, M., Schroeder, J.I., and Grossniklaus, U. (2009). Disruption of the pollen-expressed FERONIA homologs ANXUR1 and ANXUR2 triggers pollen tube discharge. Development **136:** 3279–3288.

Cai, G., and Cresti, M. (2009). Organelle motility in the pollen tube: A tale of 20 years. J. Exp. Bot. **60:** 495–508.

Chen, C.Y., Wong, E.I., Vidali, L., Estavillo, A., Hepler, P.K., Wu, H.M., and Cheung, A.Y. (2002). The regulation of actin organization by actin-depolymerizing factor in elongating pollen tubes. Plant Cell **14:** 2175–2190.

Chen, N., Qu, X., Wu, Y., and Huang, S. (2009). Regulation of actin dynamics in pollen tubes: Control of actin polymer level. J. Integr. Plant Biol. **51:** 740–750.

Cheung, A.Y., Duan, Q.H., Costa, S.S., de Graaf, B.H., Di Stilio, V.S., Feijo, J., and Wu, H.M. (2008). The dynamic pollen tube cytoskeleton: Live cell studies using actin-binding and microtubule-binding reporter proteins. Mol. Plant **1:** 686–702.

Cheung, A.Y., and Wu, H.M. (2004). Overexpression of an *Arabidopsis* formin stimulates supernumerary actin cable formation from pollen tube cell membrane. Plant Cell **16:** 257–269.

Cheung, A.Y., and Wu, H.M. (2008). Structural and signaling networks for the polar cell growth machinery in pollen tubes. Annu. Rev. Plant Biol. **59:** 547–572.

Cole, R.A., and Fowler, J.E. (2006). Polarized growth: Maintaining focus on the tip. Curr. Opin. Plant Biol. **9:** 579–588.

Crawford, B.C., and Yanofsky, M.F. (2008). The formation and function of the female reproductive tract in flowering plants. Curr. Biol. **18:** R972–R978.

Deeks, M.J., Fendrych, M., Smertenko, A., Bell, K.S., Oparka, K., Cvrcková, F., Zársky, V., and Hussey, P.J. (2010). The plant formin AtFH4 interacts with both actin and microtubules, and contains a newly identified microtubule-binding domain. J. Cell Sci. **123:** 1209–1215.

Deeks, M.J., Rodrigues, C., Dimmock, S., Ketelaar, T., Maciver, S.K., Malhó, R., and Hussey, P.J. (2007). *Arabidopsis* CAP1 - A key regulator of actin organisation and development. J. Cell Sci. **120:** 2609–2618.

Fan, X., Hou, J., Chen, X., Chaudhry, F., Staiger, C.J., and Ren, H. (2004). Identification and characterization of a Ca^{2+}-dependent actin filament-severing protein from lily pollen. Plant Physiol. **136:** 3979–3989.

Fu, Y., Wu, G., and Yang, Z. (2001). Rop GTPase-dependent dynamics of tip-localized F-actin controls tip growth in pollen tubes. J. Cell Biol. **152:** 1019–1032.

Geitmann, A., and Emons, A.M.C. (2000). The cytoskeleton in plant and fungal cell tip growth. J. Microsc. **198:** 218–245.

Gu, Y., Fu, Y., Dowd, P., Li, S., Vernoud, V., Gilroy, S., and Yang, Z. (2005). A Rho family GTPase controls actin dynamics and tip growth via two counteracting downstream pathways in pollen tubes. J. Cell Biol. **169:** 127–138.

Henty, J.L., Bledsoe, S.W., Khurana, P., Meagher, R.B., Day, B., Blanchoin, L., and Staiger, C.J. (2011). *Arabidopsis* actin depolymerizing factor4 modulates the stochastic dynamic behavior of actin filaments in the cortical array of epidermal cells. Plant Cell **23:** 3711–3726.

Higaki, T., Kutsuna, N., Sano, T., Kondo, N., and Hasezawa, S. (2010). Quantification and cluster analysis of actin cytoskeletal structures in plant cells: Role of actin bundling in stomatal movement during diurnal cycles in *Arabidopsis* guard cells. Plant J. **61:** 156–165.

Holdaway-Clarke, T.L., Feijó, J.A., Hackett, G.R., Kunkel, J.G., and Hepler, P.K. (1997). Pollen tube growth and the intracellular cytosolic calcium gradient oscillate in phase while extracellular calcium influx is delayed. Plant Cell **9:** 1999–2010.

Huang, S., Blanchoin, L., Kovar, D.R., and Staiger, C.J. (2003). *Arabidopsis* capping protein (AtCP) is a heterodimer that regulates assembly at the barbed ends of actin filaments. J. Biol. Chem. **278:** 44832–44842.

Huang, S., Jin, L., Du, J., Li, H., Zhao, Q., Ou, G., Ao, G., and Yuan, M. (2007). SB401, a pollen-specific protein from *Solanum berthaultii*, binds to and bundles microtubules and F-actin. Plant J. **51:** 406–418.

Huck, N., Moore, J.M., Federer, M., and Grossniklaus, U. (2003). The *Arabidopsis* mutant feronia disrupts the female gametophytic control of pollen tube reception. Development **130:** 2149–2159.

Kägi, C., and Gross-Hardt, R. (2007). How females become complex: Cell differentiation in the gametophyte. Curr. Opin. Plant Biol. **10:** 633–638.

Kato, M., Nagasaki-Takeuchi, N., Ide, Y., and Maeshima, M. (2010). An *Arabidopsis* hydrophilic Ca^{2+}-binding protein with a PEVK-rich domain, PCaP2, is associated with the plasma membrane and interacts with calmodulin and phosphatidylinositol phosphates. Plant Cell Physiol. **51:** 366–379.

Kovar, D.R., Drøbak, B.K., and Staiger, C.J. (2000). Maize profilin isoforms are functionally distinct. Plant Cell **12:** 583–598.

Kovar, D.R., and Pollard, T.D. (2004). Insertional assembly of actin filament barbed ends in association with formins produces piconewton forces. Proc. Natl. Acad. Sci. USA **101:** 14725–14730.

Lee, Y.J., Szumlanski, A., Nielsen, E., and Yang, Z. (2008). Rho-GTPase-dependent filamentous actin dynamics coordinate vesicle targeting and exocytosis during tip growth. J. Cell Biol. **181:** 1155–1168.

Lee, Y.J., and Yang, Z. (2008). Tip growth: Signaling in the apical dome. Curr. Opin. Plant Biol. **11:** 662–671.

Li, J., Henty-Ridilla, J.L., Huang, S., Wang, X., Blanchoin, L., and Staiger, C.J. (2012). Capping protein modulates the dynamic behavior of actin filaments in response to phosphatidic acid in *Arabidopsis*. Plant Cell **24:** 3742–3754.

Li, J., Wang, X., Qin, T., Zhang, Y., Liu, X., Sun, J., Zhou, Y., Zhu, L., Zhang, Z., Yuan, M., and Mao, T. (2011). MDP25, a novel calcium regulatory protein, mediates hypocotyl cell elongation by destabilizing cortical microtubules in *Arabidopsis*. Plant Cell **23:** 4411–4427.

Lovy-Wheeler, A., Wilsen, K.L., Baskin, T.I., and Hepler, P.K. (2005). Enhanced fixation reveals the apical cortical fringe of actin filaments as a consistent feature of the pollen tube. Planta **221:** 95–104.

Nagasaki, N., Tomioka, R., and Maeshima, M. (2008). A hydrophilic cation-binding protein of *Arabidopsis thaliana*, AtPCaP1, is localized to plasma membrane via N-myristoylation and interacts with calmodulin and the phosphatidylinositol phosphates PtdIns(3,4,5)P(3) and PtdIns (3,5)P(2). FEBS J. **275:** 2267–2282.

Picton, J.M., and Steer, M.W. (1983). Membrane recycling and the control of secretory activity in pollen tubes. J. Cell Sci. **63:** 303–310.

Pierson, E.S., Miller, D.D., Callaham, D.A., van Aken, J., Hackett, G., and Hepler, P.K. (1996). Tip-localized calcium entry fluctuates during pollen tube growth. Dev. Biol. **174:** 160–173.

Qin, Y., and Yang, Z. (2011). Rapid tip growth: Insights from pollen tubes. Semin. Cell Dev. Biol. **22:** 816–824.

Qu, X., Zhang, H., Xie, Y., Wang, J., Chen, N., and Huang, S. (2013). *Arabidopsis* villins promote actin turnover at pollen tube tips and facilitate the construction of actin collars. Plant Cell **25:** 1803–1817.

Rato, C., Monteiro, D., Hepler, P.K., and Malhó, R. (2004). Calmodulin activity and cAMP signalling modulate growth and apical secretion in pollen tubes. Plant J. **38:** 887–897.

Spudich, J.A., and Watt, S. (1971). The regulation of rabbit skeletal muscle contraction. I. Biochemical studies of the interaction of the tropomyosin-troponin complex with actin and the proteolytic fragments of myosin. J. Biol. Chem. **246:** 4866–4871.

Staiger, C.J., Poulter, N.S., Henty, J.L., Franklin-Tong, V.E., and Blanchoin, L. (2010). Regulation of actin dynamics by actin-binding proteins in pollen. J. Exp. Bot. **61:** 1969–1986.

Staiger, C.J., Sheahan, M.B., Khurana, P., Wang, X., McCurdy, D.W., and Blanchoin, L. (2009). Actin filament dynamics are dominated by rapid growth and severing activity in the *Arabidopsis* cortical array. J. Cell Biol. **184:** 269–280.

Su, H., Zhu, J., Cai, C., Pei, W., Wang, J., Dong, H., and Ren, H. (2012). FIMBRIN1 is involved in lily pollen tube growth by stabilizing the actin fringe. Plant Cell **24:** 4539–4554.

Sundaresan, V., Springer, P., Volpe, T., Haward, S., Jones, J.D., Dean, C., Ma, H., and Martienssen, R. (1995). Patterns of gene action in plant development revealed by enhancer trap and gene trap transposable elements. Genes Dev. **9:** 1797–1810.

Wang, H.J., Wan, A.R., and Jauh, G.Y. (2008). An actin-binding protein, LILIM1, mediates calcium and hydrogen regulation of actin dynamics in pollen tubes. Plant Physiol. **147:** 1619–1636.

Wu, Y., Yan, J., Zhang, R., Qu, X., Ren, S., Chen, N., and Huang, S. (2010). *Arabidopsis* FIMBRIN5, an actin bundling factor, is required for pollen germination and pollen tube growth. Plant Cell **22:** 3745–3763.

Xiang, Y., Huang, X., Wang, T., Zhang, Y., Liu, Q., Hussey, P.J., and Ren, H. (2007). ACTIN BINDING PROTEIN 29 from *Lilium* pollen plays an important role in dynamic actin remodeling. Plant Cell **19:** 1930–1946.

Yan, A., Xu, G., and Yang, Z.B. (2009). Calcium participates in feedback regulation of the oscillating ROP1 Rho GTPase in pollen tubes. Proc. Natl. Acad. Sci. USA **106:** 22002–22007.

Yang, W.C., Ye, D., Xu, J., and Sundaresan, V. (1999). The *SPOROCYTELESS* gene of *Arabidopsis* is required for initiation of sporogenesis and encodes a novel nuclear protein. Genes Dev. **13:** 2108–2117.

Yang, Z. (2008). Cell polarity signaling in *Arabidopsis*. Annu. Rev. Cell Dev. Biol. **24:** 551–575.

Ye, J., Zheng, Y., Yan, A., Chen, N., Wang, Z., Huang, S., and Yang, Z. (2009). *Arabidopsis* formin3 directs the formation of actin cables and polarized growth in pollen tubes. Plant Cell **21:** 3868–3884.

Yokota, E., Tominaga, M., Mabuchi, I., Tsuji, Y., Staiger, C.J., Oiwa, K., and Shimmen, T. (2005). Plant villin, lily P-135-ABP, possesses G-actin binding activity and accelerates the polymerization and depolymerization of actin in a Ca^{2+}-sensitive manner. Plant Cell Physiol. **46:** 1690–1703.

Zhang, H., Qu, X., Bao, C., Khurana, P., Wang, Q., Xie, Y., Zheng, Y., Chen, N., Blanchoin, L., Staiger, C.J., and Huang, S. (2010). *Arabidopsis* VILLIN5, an actin filament bundling and severing protein, is necessary for normal pollen tube growth. Plant Cell **22:** 2749–2767.

Zhu, L., Zhang, Y., Kang, E., Xu, Q., Wang, M., Rui, Y., Liu, B., Yuan, M., and Fu, Y. (2013). MAP18 regulates the direction of pollen tube growth in *Arabidopsis* by modulating F-actin organization. Plant Cell **25:** 851–867.